Available online at www.sciencedirect.com
ScienceDirect
Ceramics International 37 (2011) 927–934
CERAMICS INTERNATIONAL
www.elsevier.com/locate/ceramint

# Synergistically reinforcement of a self-setting calcium phosphate cement with bioactive glass fibers

Nader Nezafati [a], Fathollah Moztarzadeh [a], Saeed Hesaraki [b], Masoud Mozafari [a,*]

[a] *Biomaterials Group, Faculty of Biomedical Engineering (Center of Excellence), Amirkabir University of Technology, P.O. Box 15875-4413, Tehran, Iran*
[b] *Ceramic Department, Materials and Energy Research Center, Tehran, Iran*

Received 19 June 2010; received in revised form 26 October 2010; accepted 29 October 2010
Available online 3 December 2010

**Abstract**

Calcium phosphate cements (CPCs) are highly promising for clinical uses due to their *in situ*-setting ability, excellent osteoconductivity and bone-replacement capability. However, the low strength limits their uses to non-load-bearing applications. In the present research, first, bioactive glass fibers (BGFs) in the ternary $SiO_2$–CaO–$P_2O_5$ system were prepared, and then the fiber composites with compositions based on CPC and BGFs were prepared and characterized. Then, the effect of structure and amount of BGF incorporation into the CPC system, and the effect of mechanical compaction on the fiber-modified system were investigated. The results showed that the compressive strength of the set cements without any BGFs was 0.635 MPa which was optimally increased to 3.69 MPa by applying 15% BGF and then decreased by further addition of it. In addition, both the work-of-fracture and elastic modulus of the cement were considerably increased after applying the fibers in the cement composition. Also, the setting time slightly decreased by applying the fibers. In summary, processing parameters were tailored to achieve optimum mechanical properties and strength. The prepared composite may be useful in surgical sites that are not freely accessible by open surgery or when using minimally invasive techniques.


*Keywords:* B. Composite; Calcium phosphate cement; Bioactive glass fiber; Mechanical properties

## 1. Introduction

The development of CPCs has led to the production of a new class of ceramic grafting biomaterials which are mouldable and set at physiological conditions and therefore find application in non-load-bearing indications in craniofacial surgery [1], as well as in dental applications such as endodontics [2] and the repair of periodontal bone defects [3].

CPCs are also highly promising for wide clinical uses due to their self-setting ability, excellent osteoconductivity, and capability to be replaced with new bone. The first CPC was developed in 1986 [4], and it consisted of tetracalcium phosphate (TTCP, $Ca_4(PO_4)_2O$) and dicalcium phosphate anhydrous (DCPA, $CaHPO_4$) [4]. Since then, different kinds of CPCs with different compositions have been developed and characterized [5–12]. The CPC paste can intimately adapt to neighboring bone even for irregularly shaped cavities, and then harden *in situ* to form hydroxyapatite (HAp) [13–15]. Since the HAp from CPCs is formed in an aqueous environment at 37 °C, it is more similar to biological apatites than sintered HAp formed at high temperatures [15]. Therefore, CPC is highly bioactive, biocompatible and osteoconductive, and can be replaced by new bone [13–15]. As a result, CPC was approved in 1996 by the Food and Drug Administration for repairing craniofacial defects in humans, thus becoming the first CPC available for clinical use [14]. However, the low strength and susceptibility to catastrophic fracture have limited CPCs to only non-load-bearing bone repairs [13–15]. It is important to note that, the use of CPCs was ‘‘limited to the reconstruction of non-stress-bearing bone’’ [13], and unfortunately their main restriction is poor mechanical properties, so their applications are just restricted to non-loading sites. Because of the mentioned disadvantages, during the past decade, many efforts have been made to improve this deficiency. For instance, Xu and Ouinn [16] used 25 vol.% of a resorbable polymer with diameter of 322 μm in a cement matrix. They observed that the

* Corresponding author. Tel.: +98 21 22373717; fax: +98 21 22354162.
*E-mail address:* mmozafari@aut.ac.ir (M. Mozafari).

0272-8842/$36.00 
doi:10.1016/j.ceramint.2010.11.002

work-of-fracture and flexural resistance of cement were respectively increased 100 and 3 times greater than for unreinforced cements. In another study [17], the mechanical strength of bone cement was increased by entering poly(lactic-co-glycolic acid) (PLGA) microparticles in the matrix of a CPC. In this research, which was done by Link et al. [17], the composite was tested under a mechanical test (push-out) after implantation in a rat cranial defect over 4 and 8 weeks. The obtained results showed that the strength of the composite was increased significantly compared to the cement without microparticles. Fabrication of an injectable poly(propylene fumarate)/b-tricalcium phosphate paste composite was one of the next attempts to improve the mechanical properties of cement using its cross-linking characteristics [18]. Moreover, in another research, Dos Santos et al. [19] was reported the reinforcement of CPCs incorporated with polyamide fibers up to 1.6%, and fibers had a little effect on compressive strength. Another report showed that polyglactin knitted mesh on the tensile surface of CPC increased the work-of-fracture value by nearly 100 times [20]. Xu and Simon reported the use of resorbable polyglactin fibers to initially improve the flexural strength of their cement and following degradation result in the formation of macroporosity [21]. Also, Pan et al. [22] investigated the effect of chitosan fibers combined with gelatin on a CPC. It was shown that tensile strength of chitosan fiber composite was increased by 106 and 114% with the impregnation of gelatin at mass fractions of 5 and 10%. The optimal flexural strength enhancement was obtained when CPCs was reinforced with fibers at a volume fraction of 30% and a gelatin at mass fraction of 5% [22].

Among all kinds of materials as the second phase for preparing fiber composites, there is an increasing interest in the use of bioactive glass as a good choice for bone repair [23,24]. This material has a widely recognized ability to foster the growth of bone cells [25,26], and to bond strongly with hard and soft tissue [27]. Upon implantation, BGFs undergo specific reactions, leading to the formation of HAp layers, on their surfaces, which is strongly responsible for their strong bonding with surrounding tissue [28]. A sol–gel derived BGF with at least 60 mol% $SiO_2$ can develop HAp layers in a short period of time during the direct contact with a physiological solutions like simulated body fluid (SBF), whereas melt-glass with less than 55 mol% $SiO_2$ requires several days to form a polycrystalline hydroxy carbonate apatite (HCA) layer [28]. This high reactivity of sol–gel derived glasses is related to a larger volume fraction of nanometer porosity on surface, larger concentration of silanols on the surface [29] and higher surface area [30,31] than those of melt-derived glasses. All of these mentioned advantages encouraged us to apply sol–gel derived BGFs in the CPC matrix to create an optimally reinforced composite with appropriate mechanical properties.

Accordingly, the objective of the present research was to develop a mechanically strong CPC based composite reinforced with BGFs, and to investigate the effects of fiber contents on the setting time and mechanical properties. The hypothesis to be tested was the BGF volume fraction would significantly affect the setting time and mechanical properties along with excellent biocompatibility.

## 2. Materials and methods

### 2.1. Materials

For the synthesis of BGFs, tetraethylorthosilicate (TEOS: $C_8H_{20}O_4Si$) (No. 8006581000), calcium nitrate ($Ca(NO_3)_2 \cdot 4H_2O$) (No. 22384298), triethyl phosphate (TEP: $C_6H_{15}O_4P$) (No. 8211411000) and 0.1 M hydrochloric acid (HCl) were purchased from Merck Inc.

Also, dicalcium phosphate dehydrate (DCPD) (No. 2144), calcium carbonate ($CaCO_3$) (No. 2069) and disodium hydrogen phosphate ($Na_2HPO_4$) (No. 6586) were purchased from Merck Inc. to prepare the cement phase.

### 2.2. Preparation of BGFs

The sol–gel derived BGFs were prepared according to the following procedure. In short, TEOS was added to a water–ethanol solution (pH = 1.5, adjusted with HCl) at a molar ratio of 2:1 for water/TEOS and 4:1 for ethanol/TEOS. The mixture was stirred for 1 h at room temperature. The TEP was added to the silica sol, which was stirred for another 1 h. Calcium nitrate was then introduced to the sol and the mixture was stirred for an additional hour. The resultant sol was stirred at 50 rpm by concentrating the sol through solvent removal at 20 °C. The condensation process was terminated when the viscosity of the solution was sufficient for fiber pulling (until viscosities near 4–5 Pa s were achieved). The fiber-shaped gel was produced by extruding the viscous gel through a thin syringe with needle's inside diameter of 0.01 mm. Fibers were then dried for 24 h at 70 °C. Finally, they were heated to 700 °C at an approximate rate of 3 K $min^{-1}$ and sintered and stabilized at 700 °C for 24 h.

### 2.3. Preparation of CPC

First, TTCP powder was synthesized by a combination of 1 mole of DCPD and 1 mole of $CaCO_3$ after milling for 2 h. Then, it was heated to 1500 °C (in an alumina crucible) at an approximate rate of 7 K $min^{-1}$ and maintained for 5 h at the same temperature. After that, it was extracted immediately, cooled at a medium temperature and ground in a planetary mill to an average particle size of 12 μm (Fritsch particle sizer analysette 22). A mixture of DCPD (average particle size of 6 μm) and TTCP, in a molar ratio of 1:1, was used as the solid phase of the cement. The liquid phase was a solution of 6 wt% $Na_2HPO_4$. The cement paste was made by mixing the powder to the liquid phase at powder to liquid ratio of 3 g/ml.

### 2.4. Preparation of CPC/BGF composites

To prepare CPC/BGF composites, the obtained BGFs were mixed with the cement powder at various weight ratios of 5, 15 and 25% (based on the whole weight of the powder and liquid)

and then the liquid phase was added to the mixture to obtain a paste. Note that the weight of the glassy fibers was not considered in the powder-to-liquid (P/L) calculations.

### 2.5. Sample characterization

#### 2.5.1. DSC and TGA analyses

The DSC and TGA curves were obtained in a Shimadzu DSC-50 and a Shimadzu TGA-50 apparatuses, respectively, under a nitrogen atmosphere that starting from room temperature up to 1000 °C with the heating rate of 5 °C/min.

#### 2.5.2. XRD analysis

The compositions of sample were analyzed by XRD with Philips PW3710 diffractometer. This instrument works with voltage and current settings of 40 kV and 30 mA, respectively and uses Cu-Ka radiation (1.540600 Å). For qualitative analysis, XRD diagrams were recorded in the interval $10^\circ \leq 2\theta \leq 50^\circ$ at scan speed of 2°/min being the step size 0.02° and the step time 1 s.

#### 2.5.3. SEM analysis

The morphology and microstructure of the synthesized samples were evaluated using SEM. The samples were coated with a thin layer of gold (Au) by sputtering (EMITECH K450X, England) and then the morphology of them were observed on a SEM (Seron Technology, AIS-2100) that operated at the acceleration voltage of 30 kV.

#### 2.5.4. EDX analysis

Energy dispersive X-ray analyzer (EDX, Rontec, Germany) directly connected to SEM was used to investigate semi-quantitatively chemical compositions.

#### 2.5.5. FTIR analysis

The samples were examined by FTIR with Bomem MB 100 spectrometer. For IR analysis, in first 1 mg of the scraped samples were carefully mixed with 300 mg of KBr (infrared grade) and pelletized under vacuum. Then, the pellets were analyzed at the scan speed of 23 Scan/min with 4 $cm^{-1}$ resolution.

#### 2.5.6. Setting time

The setting time of cements was measured in accordance with the ASTM C266-89 standard method using a Gillmore needle test with a needle weight of 113.4 g and tip diameter of 2.13 mm. In the test method, the paste was considered to set when the needle could not form a visual print onto the surfaces of the sample.

#### 2.5.7. Mechanical behavior

The mechanical behavior of prepared composites was investigated by conducting compressive strength test. The cylindrical specimens were formed in Teflon mould (6 mm in diameter and 12 mm in height), and the thickness was measured by an electric digital caliper. Then, specimens stored in an incubator (100% humidity and 37 °C) for 24 h and the compressive strengths of the wet samples were measured by a Zwick/Roell Universal Testing Machine apparatus with a crosshead speed of 1 mm/min. The following equations were used for the calculation of $E$ (Young's modulus) (1) and $\sigma$ (ultimate compressive stress) (2):

$$E = \frac{KL}{A} \tag{1}$$

$$\sigma = \frac{F}{A} \tag{2}$$

where $F$ is the ultimate load; $K$ is the stiffness; $L$ is the length of sample; $A$ is the average of surface area calculated from the following Eq. (3):

$$A = \frac{\pi}{2} \times \frac{1}{4}(d_1^2 + d_1^2) \tag{3}$$

where $d_1$ and $d_2$ are the diameters of the bases of the cylindrical samples. The $K$ value is calculated by the slope of the load–displacement curve at the fracture point. The work-of-fracture (energy absorbed by the sample before the fracture) was obtained from the area under the load–displacement curve normalized by the specimen's cross-sectional area.

### 2.6. Statistical analysis

All the experiments were performed in fifth replicate. The results were given as means ± standard error (SE). Statistical analysis was performed by using One-way ANOVA and Tukey test with significance reported when $P < 0.05$. Also, for investigation of group normalizing, Kolmogorov–Smirnov test was used.

## 3. Results and discussions

### 3.1. Thermal analyses of the prepared BGF

The DSC and TGA analyses of the BGFs were carried out to obtain the right sintering temperature which is shown in Fig. 1. The first endothermic peak, which initiated at 110 °C,

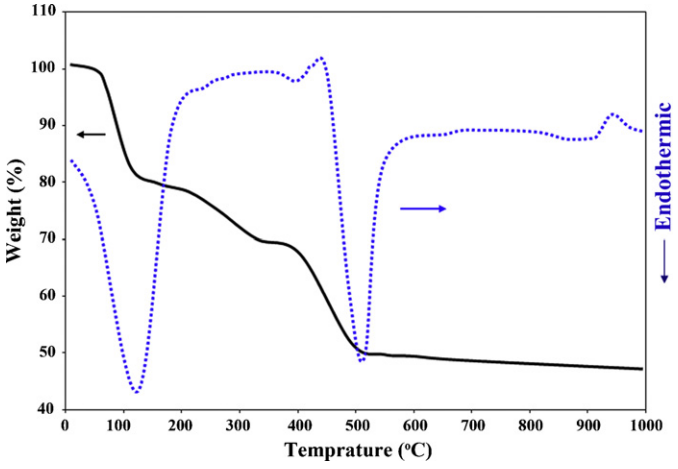


Fig. 1. The DSC and TGA analyses of the prepared BGFs.

corresponds to the release of physically adsorbed water that was not removed during drying. The TGA trace showed that all water and by-products from the polycondensation reaction were removed between 85 °C and 150 °C (17% weight loss). Two other endothermic peaks, starting at 390 °C, corresponds to the pyrolysis reaction of free organic species and/or the release of the resulting water from the further condensation of silanol and P–OH groups and the removal of nitrate groups that are usually removed in the thermal stabilization process [32]. The removal of species at these temperatures is reflected in the weight loss trace from TGA. All nitrates were removed by 530 °C (a further 27% of the total weight loss), so the total weight loss was 44%. Finally, the exothermic peak around 970 °C is attributed to the crystallization process of $CaSiO_3$ (β-wollastonite) and cristobalite ($SiO_2$) [32], which has been found to form at higher temperatures in similar glasses [33,34]. Also, a small endothermic DSC peak centralized at about 990 °C implies that the material was fully crystalline at above 1000 °C. No significant weight loss was observed above 700 °C, also these curves confirmed that the residuals could be removed before 700 °C, thus this temperature is appropriate for a fully stabilization of the structure. It is important to point out that the obtained thermal results for the prepared BGF is the same as the results reported by Mozafari et al. [35] who worked on the synthesis and characterization of bioactive glass nanopowder with this compositional structure, which shows the accuracy of the test. Subsequently, the prepared sample was treated at 700 °C during 24 h for stabilization. Thereupon, the XRD pattern of the prepared BGFs after stabilization did not contain diffraction maxima, indicative of the internal disorder and the glassy nature of the BGF which is shown in Fig. 2(a).

### 3.2. XRD analysis

The phase purity and phase structure of the synthesized BGF, the CPC (unreinforced cement) and the CPC/BGF composite with 15% BGF were characterized by XRD which are shown in Fig. 2. In the BGF pattern, the sample almost takes amorphous state which indicates the internal disorder and glassy nature of these materials. It is worth mentioning that the BGF sample does not show any crystalline states [35].

For both unreinforced CPC and CPC/BGF samples a considerable amount of the reactant phase in the cement composition is observed. The apatite phase is also observed in the compositions (apatite is the product of the setting reaction). It is seen that the BGFs never prevent the conversion of reactant materials (TTCP and DCPD) to apatite phase.

According to the previous explanations, the setting mechanisms of CPCs are so complicated that have not been identified completely but there are some hypotheses about setting phenomena. The main reason for the setting process of CPCs is the precipitation of different phases such as brushite, apatite or octacalcium phosphate in the cement paste [36]. Herein, brushite and TTCP can also be seen in the XRD patterns. It is also notable that, the patterns of former composites by other researchers were very similar to that of presented here too.

### 3.3. SEM observations and EDX analysis

SEM is a powerful tool for observing the morphology and size of different samples. Herein, after the reaction was stopped at a specific time in each sample, the surfaces of the samples was gold sputtered, and then observed by SEM. Fig. 3(a) shows a typical SEM micrograph of a BGF produced by extruding the gel composition. This figure indicated that the diameter of the synthesized BGF is less than 20 μm. In addition, EDX analysis as an effective method to investigate semi-quantitatively chemical compositions was used. Fig. 3(b) shows the EDX spectra of the BGF. The EDX spectrum shows the peaks of Si, P, Ca, and O which are the main components of the prepared BGF. It is also notable that the presence of gold (Au) on the surface of BGF was only related to the sputtering before SEM analysis.

Fig. 4(a) and (b) shows the high and low magnifications of the prepared composite containing 15% BGF, respectively, to confirm that the BGFs were incorporated into the CPC matrix.

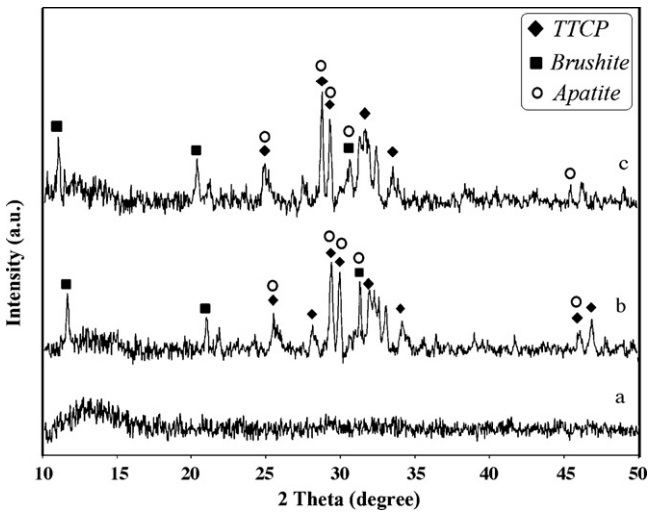


Fig. 2. The XRD patterns of (a) the prepared BGFs, (b) the CPC (unreinforced cement) and (c) the CPC/BGF composite with 15% BGF.

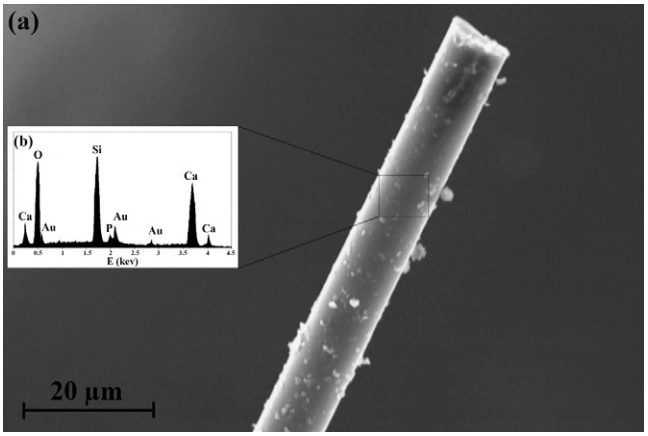


Fig. 3. The typical SEM micrograph of (a) BGF and (b) the EDX spectra of the BGF.

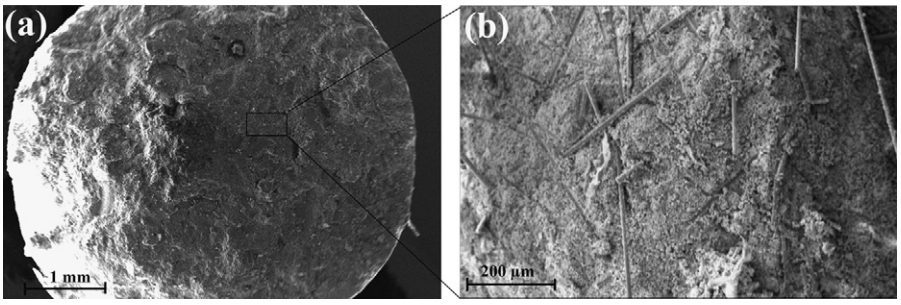


Fig. 4. The low and high magnifications of the prepared composite containing 15% BGF (a) and (b), respectively.

Some dispersed particles of the glass phase (which is probably due to crushing of the BGFs) are also observed.

### 3.4. FTIR analysis

Fig. 5 shows the FTIR absorbance spectra of different scraped material surfaces. The FTIR spectrum of fiber-free CPC sample showed some significant peaks. The existence of P–O stretching band at around 600 and 1000 $cm^{-1}$ indicated the presence of calcium phosphate contents. Similarly, the peak assignments for other wavenumbers are as follows: band around 3419, hydroxyl stretch; 1613, hydroxyl $\nu_3$; 883, carbonate $\nu_2$; 1430 and 1600, carbonate $\nu_3$; 1016, phosphate $\nu_3$; 660, 630 and 580, phosphate $\nu_4$ [37].

The FTIR spectrum of the BGF exhibited five infrared bands located at around: 600, 800, 922, 1066 and 1250 $cm^{-1}$. These bands, those positioned at 800, 922, 1120 and 1218 $cm^{-1}$ are related to the silicate network and respectively ascribed to the Si–O symmetric stretching of bridging oxygen atoms between tetrahedrons, Si–O stretching of non-bridging oxygen atoms, Si–O–Si symmetric stretching, and the Si–O–Si asymmetric stretching. The bands located at around 600 $cm^{-1}$ are attributed to the asymmetric vibration of $PO_4^{3-}$ [38–40]. The band at 1000 $cm^{-1}$ arises from $\upsilon_3$ $PO_4$ and the bond at 603 arises from $\upsilon_4$ $PO_4$ [41]. Also, some carbonate content was observed around 870 and 1645 $cm^{-1}$, which are indications for the presence of carbonate groups due to incubation in incubator at 37 °C and relative humidity of 100% in $CO_2$ atmosphere for 24 h. These related carbonate bands can also be seen for all samples. Two bonds were also observed for all the composite samples at around 3500 and 620 $cm^{-1}$ due to the stretching mode of hydrogen-bonded $OH^-$ ions and liberational mode of hydrogen-bonded $OH^-$ ions, respectively [42].

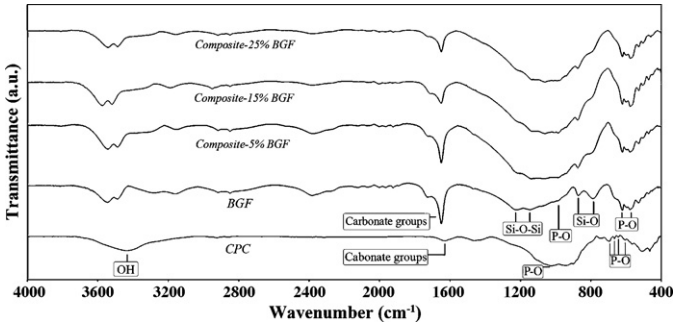


Fig. 5. The FTIR absorbance spectra of different samples.

### 3.5. Setting time

The powder and the liquid components were mixed together with L/P ratio of 0.33 ml $g^{-1}$. Next, the cement paste was cast into steel dies, and setting time measurements performed by Gilmore needle. According to the results given in Fig. 6, the initial setting time of the fiber-free CPC (control) was about 20 min, which was not significantly different that of the composite with 5% BGFs. In contrast, the setting time of composites with 15% and 25% BGFs were lower than the control sample. The setting mechanism of CPC is based on acidic and basic reactions. This process is so complicated which has not been identified completely but there are some hypotheses about the setting phenomena of these cements. The main reason for the setting process of CPCs is the precipitation of different phases such as brushite, apatite or octacalcium phosphate in the cement paste [36]. In apatitic CPCs, the presence of the initial crystals of apatite is due to the dissolution of TTCP particles and their hydrolysis to stoichiometric hydroxyl apatite as follows (4):

$$Ca_4(PO_4)_2 + H_2O \rightarrow Ca_{10}(PO_4)_6(OH)_2 + Ca(OH)_2 \quad (4)$$

In addition, the growth of apatite crystals is because of the acidic-basic reaction which is shown below (5) [36]:

$$3Ca_4(PO_4)_2O + 6CaHPO_4 \rightarrow 2Ca_2(HPO_4)(PO_4)_5OH + H_2O \quad (5)$$

There are different parameters which affect the setting time of CPCs and consequently increase their strength, including the

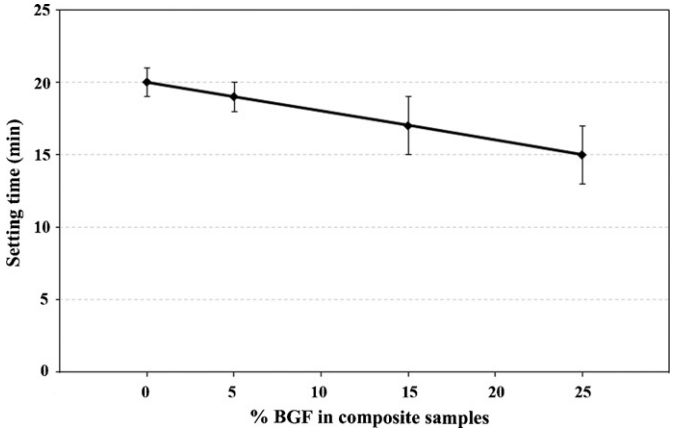


Fig. 6. The initial setting time of different samples.

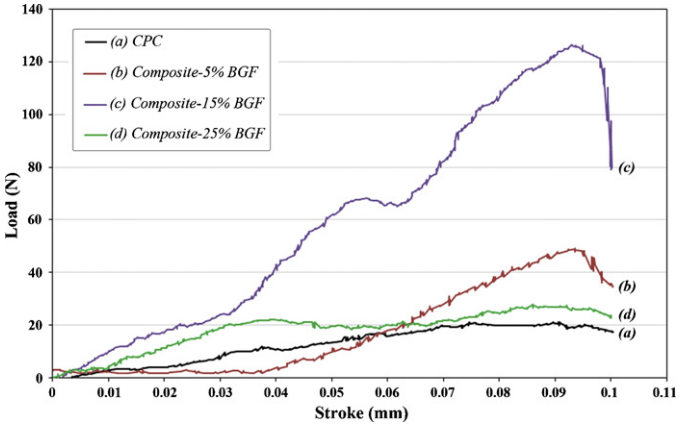


Fig. 7. The load displacement curves of the prepared CPC sample and the composites containing 5, 15 and 25% BGFs.

composition of material used in the liquid/solid phase, the powder-to-liquid ratio and particle size of the reactants [43]. Herein, the higher powder-to-liquid ratio of the BGF-containing CPCs (especially higher concentrations of BGFs) suggested that it is the main reason for decreasing the initial setting time of the composites.

### 3.6. Mechanical properties

Fiber-reinforced composites have very high strength to weight and stiffness to weight ratios. On the other hand, they show excellent durability and corrosion resistance, good fatigue behavior and dimensional stability. Fibers can be in continuous or discontinuous forms. This investigation focused on randomly distributed, discontinuous BGF reinforced CPC composites. One significant difference between the properties of random discontinuous fiber composites and those of unidirectional continuous fiber reinforced composites is that the mechanical properties of the former reaches a maximum as the fiber volume fraction increases and then start to decrease. For the latter, the mechanical properties increase with the fiber volume fraction [44]. The fiber volume fraction at which the highest mechanical properties are achieved is of great interest for the random fiber composites. This optimal fiber volume fraction varies for different types of composites [45].

Fig. 7 shows the load displacement curves of the prepared CPC sample and the composites containing 5, 15 and 25% BGFs. The areas below the curves are a measure of the fracture (the energy required to fracture the specimen, obtained from the area under the load–displacement curve normalized by the specimen's cross-sectional area). According to this figure, it is worth mentioning that the fracture energy for the reinforced cement containing 15% BGFs was significantly higher than the control sample (un-reinforced CPC).

Herein, the compressive strength, Young's modulus and work-of-fracture properties of the composites reinforced with different amount of BGFs were also compared to the control sample which is shown in Fig. 8. The compressive strength, Young's modulus and work-of-fracture values of the composites containing 5 and 15% BGFs were considerably higher than

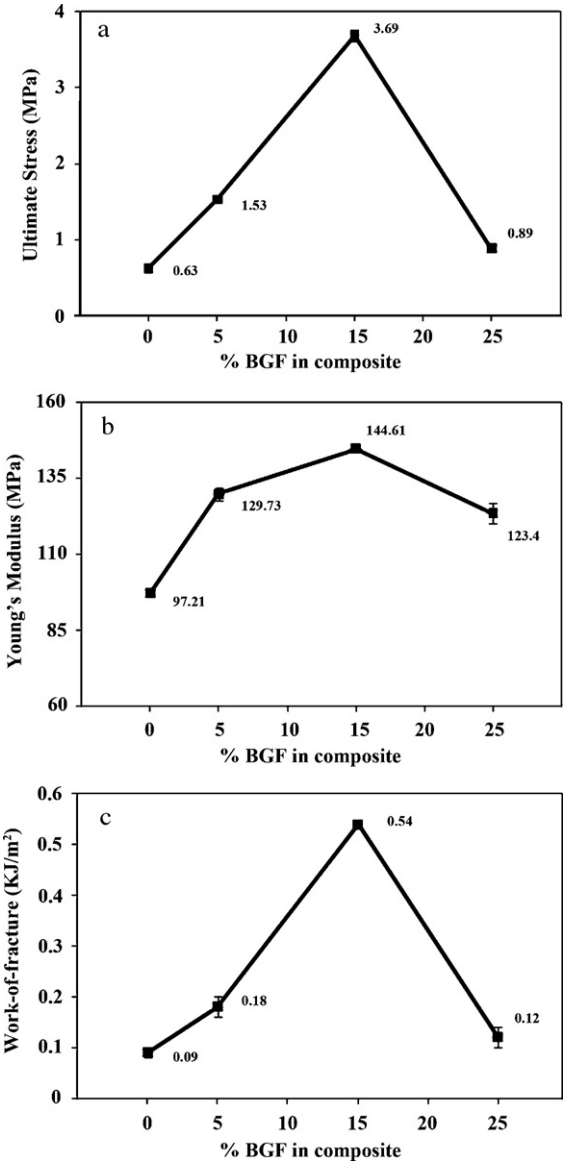


Fig. 8. The mechanical properties of composites, (a) compressive strength, (b) Young's modulus and (c) work-of-fracture values.

that of the un-reinforced cement while the values of the composite containing 25% BGFs were significantly lower than that of 5% BGFs. It can be also observed that applying the larger amounts of admixture not only increased the mechanical properties of CPC but also act as defect sites in the cement's microstructure and caused decreasing of mechanical characteristics of the samples. It is important to point out the mechanical properties of the composite samples is generally higher than the un-reinforced cement (control sample).

Basically, as a fundamental rule, unlike unidirectional fiber-reinforced composites whose mechanical properties show a continuous increase with an increase in fiber volume fraction, the modulus and strength of the random fiber composites increase with fiber volume fraction up to a certain maximum value and then start to decrease.

Mechanical properties of fiber composites are affected by their microstructures. Fig. 9 shows a SEM micrograph of the


Fig. 9. The SEM micrograph of the fractured composite sample containing 25% BGF after compression test.

fracture composite sample containing 25% BGF after compression test.

One reason for the decrease in mechanical properties at high fiber volume fraction shown in Fig. 8 is the interactions between the BGFs. Since the BGFs in the prepared composites have a random distribution, interactions between the BGFs are inevitable. When the BGFs volume fraction is low, they play the role of reinforcement. This is why below a certain fiber volume fraction, the compressive strength, Young's modulus and work-of-fracture of the composite increase with increasing. As the BGF volume fraction becomes higher, there will be more interaction between the BGFs (which has been shown in Fig. 9 with white arrows), which may lead to voids and poor bonding between the BGFs and the composites. Hence, the mechanical properties start to decrease as fiber volume fraction increases above a critical value.

According to Hesaraki et al. [46], the mechanical strength of CPCs also highly depends on the particle size distribution of the powder. In addition, the crystallinity degree of the formed apatite crystals affects this property so that decreasing the crystallite size causes more entanglement and density in the crystalline structure, and thus the strength will increase.

In this research, the prepared CPC with a known reactant particle size was used. The mechanisms which caused increasing the work-of-fracture and prevent flaw growth by adding BGFs have been suggested as follows:

- the BGFs bridge the cracks to resist their further opening and propagation;
- multiple cracking of the matrix consume the applied work in creating new surfaces;
- frictional sliding and stretching of the BGFs during pullout prevent flaw growth [47,48].

Factors such as the type and shape of the fibers can also affect the work-of-fracture and strength of ceramic composites reinforced by fibers. This means that factor(s) which cause(s) an increase composite strength would have positive effects on the work-of-fracture.

## 4. Conclusion

In conclusion, the experiments provide data to support the use of the CPC/BGF composite in bone repair applications. One of the main objectives of this study was to find the BGF volume fraction at which the BGF/CPC composites have the highest mechanical properties. Here, a CPC with improved mechanical properties was prepared by incorporating sol–gel derived BGFs. The optimum amount of fibers which successfully improved the compressive strength, modulus and toughness of the CPC was 15 wt% based on the total weight of the cement powder and liquid. It is also obvious that the applying CPC/BGF composite is notable from different points of view including improved mechanical properties, biocompatibility and bioactivity.

## References

[1] W.E. Brown, L.C. Chow, Dental restoration cement pastes, US Patent 4518430, 1985.
[2] C.D. Friedman, P.D. Costantino, S. Takagi, L.C. Chow, BoneSource hydroxyapatite cement: a novel biomaterial for craniofacial skeletal tissue engineering and reconstruction, J. Biomed. Mater. Res. (Appl. Biomater.) 43 (1998) 428–432.
[3] G.D. Brown, B.L. Mealey, P.V. Nummikoski, S.L. Bifano, T.C. Waldrop, Hydroxyapatite cement implant for regeneration of periodontal osseous defects in humans, J. Periodontol. 69 (1998) 145–157.
[4] W.E. Brown, L.C. Chow, A new calcium phosphate water setting cement, in: P.W. Brown (Ed.), Cements Research Progress, American Ceramic Society, Westerville, OH, 1986, pp. 352–379.
[5] M.P. Ginebra, E. Fernandez, E.A.P. De Maeyer, R.M.H. Verbeeck, M.G. Boltong, J. Ginebra, F.C.M. Driessens, J.A. Planell, Setting reaction and hardening of an apatite calcium phosphate cement, J. Dent. Res. 76 (1997) 905–912.
[6] K. Ishikawa, Y. Miyamoto, M. Takechi, T. Toh, M. Kon, M. Nagayama, K. Asaoka, Non-decay type fast-setting calcium phosphate cement: hydroxyapatite putty containing an increased amount of sodium alginate, J. Biomed. Mater. Res. 36A (1997) 393.
[7] C. Durucan, P.W. Brown, Low temperature formation of calcium deficient hydroxyapatite-PLA/PLGA composites, J. Biomed. Mater. Res. 51A (2000) 717–725.
[8] A. Yokoyama, S. Yamamoto, T. Kawasaki, T. Kohgo, M. Nakasu, Development of calcium phosphate cement using chitosan and citric acid for bone substitute materials, Biomaterials 23 (2002) 1091–1101.
[9] L.M. Grover, J.C. Knowles, G.J.P. Fleming, J.E. Barralet, In vitro ageing of brushite calcium phosphate cement, Biomaterials 24 (2003) 4133–4141.
[10] M. Bohner, G. Baroud, Injectability of calcium phosphate pastes, Biomaterials 26 (2005) 1553–1563.
[11] E. Fernández, S. Sarda, M. Hcu, M.D. Vlad, M. Gel, S. Valls, R. Torres, J. Lopez, High strength apatitic cement by modification with super plasticizers, Biomaterials 26 (2005) 2289–2296.
[12] M. Julien, I. Khairoun, R.Z. LeGeros, S. Delplace, P. Pilet, P. Weiss, G. Daculsi, J.M. Bouler, J. Guicheux, Physico-chemical-mechanical and in vitro biological properties of calcium phosphate cements with doped amorphous calcium phosphates, Biomaterials 28 (2007) 956–965.
[13] P.D. Costantino, C.D. Friedman, K. Jones, L.C. Chow, G.A. Sisson, Experimental hydroxyapatite cement cranioplasty, Plast. Reconstr. Surg. 90 (1992) 174–191.
[14] C.D. Friedman, P.D. Costantino, S. Takagi, L.C. Chow, BoneSource™ hydroxyapatite cement: a novel biomaterial for craniofacial skeletal tissue engineering and reconstruction, J. Biomed. Mater. Res. (Appl. Biomater.) 43B (1998) 428–432.

[15] L.C. Chow, Calcium phosphate cements: chemistry, properties and applications, Mater. Res. Symp. Proc. 599 (2000) 27–37.
[16] H.H.K. Xu, J.B. Quinn, Calcium phosphate cement containing resorbable fibers for short-term reinforcement and macroporosity, Biomaterials 23 (2002) 193–202.
[17] D.P. Link, J. Van den Dolder, J. Van den Beucken, J.G. Wolke, A.G. Mikos, J.A. Jansen, Mechanical evaluation of implanted calcium phosphate cement incorporated with PLGA microparticles, Biomaterials 27 (2006) 4941–4947.
[18] S.J. Peter, P. Kim, A.W. Yasko, M.J. Yaszemski, A.G. Mikos, Crosslinking characteristics of an injectable poly(propylene fumarate)/b-tricalcium phosphate paste and mechanical properties of the cross-linked composite for use as a biodegradable bone cement, J. Biomed. Mater. Res. 44 (1999) 314–321.
[19] L.A. dos Santos, L.C. de Oliveira, E.C.D. Rigo, R.G. Carrodeguas, A.O. Boschi, A.C.F. de Arruda, Fiber reinforced calcium phosphate cement, Artif. Organs 24 (2000) 212–216.
[20] H.H.K. Xu, F.C. Eichmiller, A.A. Giuseppetti, Reinforcement of a self-setting calcium phosphate cement with different fibers, J. Biomed. Mater. Res. 52 (2000) 107–114.
[21] H.H.K. Xu, C.G. Simon, Self-hardening calcium phosphate cementmesh composite: reinforcement, macropores and cell response, J. Biomed. Mater. Res. 69A (2004) 267–278.
[22] Z. Pan, P. Jiang, Q. Fan, Mechanical and biocompatible influences of chitosan fiber and gelatin on calcium phosphate cement, J. Biomed. Mater. Res. 82B (2007) 246–252.
[23] L.L. Hench, J. Wilson, Introduction to Bioceramics, World Scientific, Singapore, 1993.
[24] S.H. Li, J.R. De Wijn, P. Layrolle, K. de Groot, Synthesis of macroporous hydroxyapatite scaffolds for tissue engineering, J. Biomed. Mater. Res. 61 (2002) 109–120.
[25] L.L. Hench, J. Wilson, Clinical Perfomance of Skeletal Prostheses, Chapman and Hall, London, 1996.
[26] W. Cao, L.L. Hench, Bioactive Materials, Ceram. Int. 22 (1996) 493–507.
[27] M. Navarro, M.P. Ginebra, J.A. Planell, Cellular response to calcium phosphate glasses with controlled solubility, J. Biomed. Mater. Res. 67A (2003) 1009–1015.
[28] J.M. Polak, L.L. Hench, P. Kemp, Future strategies for tissue and organ replacement, in: L.L. Hench, J.R. Jones, P. Sepulveda (Eds.), Bioactive Materials for Tissue Engineering Scaffolds, Imperial College Press, London, 2002, pp. 1–22.
[29] L.L. Hench, The challenge of orthopaedic materials, Curr. Orthop. 14 (2000) 7–15.
[30] L.L. Hench, J.K. West, Biological applications of bioactive glasses, Life Chem. Rep. 13 (1996) 187–241.
[31] M. Mozafari, F. Moztarzadeh, M. Rabiee, M. Azami, N. Nezafati, Z. Moztarzadeh, M. Tahriri, Development of 3D bioactive nanocomposite scaffolds made from gelatin and nano bioactive glass for biomedical applications, Adv. Compos. Lett. 19 (2010) 91–96.
[32] P. Saravanapavan, J.R. Jones, R.S. Pryce, L.L. Hench, Bioactivity of gel-glass powders in the $CaO–SiO_2$ system: a comparison with ternary ($CaO–P_2O_5–SiO_2$) and quaternary glasses ($SiO_2–CaO–P_2O_5–Na_2O$), J. Biomed. Mater. Res. A 66 (2003) 110–119.
[33] J.R. Jonesa, L.M. Ehrenfried, L.L. Hench, Optimising bioactive glass scaffolds for bone tissue engineering, Biomaterials 27 (2006) 964–973.
[34] D.C. Greenspan, J.P. Zhong, G.P. LaTorre, Effect of surface area to volume ratio on in vitro surface reactions of bioactive glass particulates, in: O.H. Andersson, A. Yli-Urpo (Eds.), Bioceramics, vol. 7, 1994, pp. 28–33.
[35] M. Mozafari, F. Moztarzadeh, M. Tahriri, Investigation of the physico-chemical reactivity of a mesoporous bioactive $SiO_2–CaO–P_2O_5$ glass in simulated body fluid, J. Non-Cryst. Solids 356 (2010) 1470–1478.
[36] S. Hesaraki, F. Moztarzadeh, D. Sharifi, Formation of interconnected macropores in apatitic calcium phosphate bone cement with the use of an effervescent additive, J. Biomed. Mater. Res. 83 (2007) 80–87.
[37] I. Rehman, W. Bonfield, Bioceramics, vol. 8, Elsevier Science, Oxford, 1995, p. 163.
[38] V.C. Farmer, The Infrared Spectra of Minerals, Mineralogical Society, London, 1974.
[39] C.Y. Kim, A.E. Clark, L.L. Hench, Compositional dependence of calcium phosphate layer formation in fluoride bioglass, J. Biomed. Mater. Res. 26 (1992) 1147–1161.
[40] B. Smith, Infrared Spectra Interpretation. A Systematic Approach, CRC Press, Boca Raton, FL, 1999.
[41] N. Rameshbabu, T.S.S. Kumar, K. Prasad Rao, Synthesis of nanocrystalline fluorinated hydroxyapatite by microwave processing and its in vitro dissolution study, Bull. Mater. Sci. 29 (2006) 611–615.
[42] M. Mozafari, F. Moztarzadeh, M. Rabiee, M. Azami, S. Maleknia, M. Tahriri, Z. Moztarzadeh, N. Nezafati, Development of macroporous nanocomposite scaffolds of gelatin/bioactive glass prepared through layer solvent casting combined with lamination technique for bone tissue engineering, Ceram. Int. 36 (2010) 2431–2439.
[43] M. Komath, K.H. Varma, R. Sivakumar, On the development of an apatitic calcium phosphate bone cement, Bull. Mater. Sci. 23 (2000) 135–140.
[44] C. Qin, N. Soykeabkaew, N. Xiuyuan, T. Peijs, The effect of fibre volume fraction and mercerization on the properties of all-cellulose composites, Carbohydr. Polym. 71 (2008) 458–467.
[45] S.K. Garkhail, R.W.H. Heijenrath, T. Peijs, Mechanical properties of natural-fibre-mat-reinforced thermoplastics based on flax fibres and polypropylene, Appl. Compos. Mater. 7 (2000) 351–372.
[46] S. Hesaraki, A. Zamanian, F. Moztarzadeh, The influence of the acidic component of the gas-foaming porogen used in preparing an injectable porous calcium phosphate cement on its properties: acetic acid versus citric acid, J. Biomed. Mater. Res. 86B (2007) 208–216.
[47] S. Hesaraki, F. Moztarzadeh, M. Solati-Hashjin, Phase evaluation of an effervescent-added apatitic calcium phosphate bone cement, J. Biomed. Mater. Res. 79B (2006) 203–209.
[48] N. Nezafati, F. Moztarzadeh, S. Hesaraki, Evaluation of a prepared sol–gel bioactive glass fiber-reinforced calcium phosphate cement, J. Ceram. Process. Res. 10 (2010) 367–371.